Opposite hemispheric asymmetries during the ionospheric storm of 29-31 August 2004

Elvira Astafyeva, Irina Zakharenkova, Eelco Doornbos

AGU PUBLICATIONS

JGR

Journal of Geophysical Research: Space Physics

RESEARCH ARTICLE
10.1002/2014JA020710

Key Points:
- Multi-instrumental analysis of the geomagnetic storm of 29–31 August 2004
- We observe opposite hemispheric asymmetries in F layer and topside ionosphere
- Strong thermospheric and ionospheric effects occurred in the postsunset sector

Correspondence to:
E. Astafyeva,
astafyeva@ipgp.fr

Citation:
Astafyeva, E., I. Zakharenkova, and E. Doornbos (2015), Opposite hemispheric asymmetries during the ionospheric storm of 29–31 August 2004, *J. Geophys. Res. Space Physics*, *120*, 697–714, doi:10.1002/2014JA020710.

Received 8 OCT 2014
Accepted 8 DEC 2014
Accepted article online 12 DEC 2014
Published online 21 JAN 2015

Opposite hemispheric asymmetries during the ionospheric storm of 29–31 August 2004

Elvira Astafyeva[1], Irina Zakharenkova[1,2], and Eelco Doornbos[3]

[1]Institut de Physique du Globe de Paris, Paris Sorbonne Cité, Université Paris Diderot, UMR CNRS 7154, Paris, France, [2]On leave from IZMIRAN, Kaliningrad, Russia, [3]Department of Space Engineering, Delft University of Technology, Delft, Netherlands

Abstract By making use of multiple ground-based and spaceborne instruments, we study ionospheric and thermospheric behavior during the moderately intense geomagnetic storm of 29–31 August 2004 (minimum *Dst* excursion of −128 nT). Although this storm was far from the strongest in solar cycle 23, it provoked quite interesting effects in the ionosphere, such as opposite hemispheric asymmetries in the ionospheric *F* layer and in the topside ionosphere and a development of the ionospheric superfountain effect in the postsunset sector. Data from ground-based GPS receivers and ionosondes revealed large increase in total electron content (TEC) and in N_mF_2 in the southern hemisphere, whereas in the northern hemisphere, very weak or no effect was observed. On the contrary, the topside measurements indicated the occurrence of a positive storm in the northern hemisphere. Overall, the strongest storm time disturbances were observed in the postsunset sector (~20:30–21:30 LT), where satellite radar altimeters TOPEX and Jason 1, along with the CHAMP satellite showed ~250–400% TEC increase in the middle- and low-latitude regions. The signatures of the ionospheric plasma enhancement were seen up to the height of the Defense Meteorological Satellite Program (DMSP) satellites (~840 km). As for the thermospheric storm, data of the Gravity Recovery and Climate Experiment (GRACE) satellite mission revealed no asymmetry in neutral density data in the evening sector (~17 UT); however, very strong hemispheric asymmetry was observed in the postsunset sector by CHAMP (~21 UT). Overall, neutral density increase in the postsunset sector was found to be much stronger than in the evening sector.

1. Introduction

Geomagnetic storms are strong disturbances in the Earth's magnetosphere due to changes in the solar wind and interplanetary magnetic field (IMF). The ionospheric response to a geomagnetic storm, which is commonly referred to as an ionospheric storm, is not yet completely understood and remains one of the primary subjects of ionospheric science [e.g., *Vlasov et al.*, 2003; *Kelley et al.*, 2004; *Tsurutani et al.*, 2004, 2006, 2008; *Mannucci et al.*, 2005, 2008, 2014; *Yizengaw et al.*, 2005, 2006; *Abdu et al.*, 2006; *Foster and Coster*, 2007; *Goncharenko et al.*, 2007; *Astafyeva et al.*, 2008; *Lu et al.*, 2008, 2012; *Zakharenkova et al.*, 2012]. An ionospheric storm is a global phenomenon, it extends to all latitudinal regions and both dayside and nightside hemispheres of the Earth, and affects all branches of telecommunication and navigation [e.g., *Pi et al.*, 1997; *Jakowski et al.*, 2005; *Basu et al.*, 2008; *Rama Rao et al.*, 2009; *Astafyeva et al.*, 2014].

Geomagnetic disturbances begin with the arrival of solar/interplanetary plasma at high velocity at Earth's magnetopause. The most significant geomagnetic and ionospheric effects are caused by hot plasma with a negative IMF B_z component, which sets up interconnection with Earth's magnetic field lines and leads to a large amount of energy deposition into the high-latitude regions of the Earth. Such high-latitude heating, in turn, can create strong dawn-to-dusk disturbance dynamo electric fields [*Blanc and Richmond*, 1980; *Richmond and Lu*, 2000; *Yizengaw et al.*, 2005; *Fejer et al.*, 2007] and expand the thermosphere, causing storm time meridional neutral winds [*Sica and Schunk*, 1990; *Fuller-Rowell et al.*, 1994; *Liu et al.*, 2005; *Lu et al.*, 2008, 2012; *Fuller-Rowell*, 2011] and generating traveling atmospheric disturbances (TADs) [*Fuller-Rowell et al.*, 1994; *Richmond and Lu*, 2000; *Paznukhov et al.*, 2009]. The high-latitude ionospheric electric fields promptly penetrate to low latitudes during the main phase of the storms [e.g., *Kikuchi et al.*, 1978, 2008; *Huang et al.*, 2005a]. These electric fields known as prompt penetration electric fields (PPEFs) are directed eastward (dawn to dusk) on the dayside and westward (dusk to dawn) on the nightside [e.g., *Kelley et al.*, 2003; *Tsurutani et al.*, 2006, 2008]. PPEF significantly affect the midlatitude and low-latitude ionosphere, being a primary cause of a dayside positive storm [e.g., *Huang et al.*, 2005b] and an overall enhancement of the dayside total electron

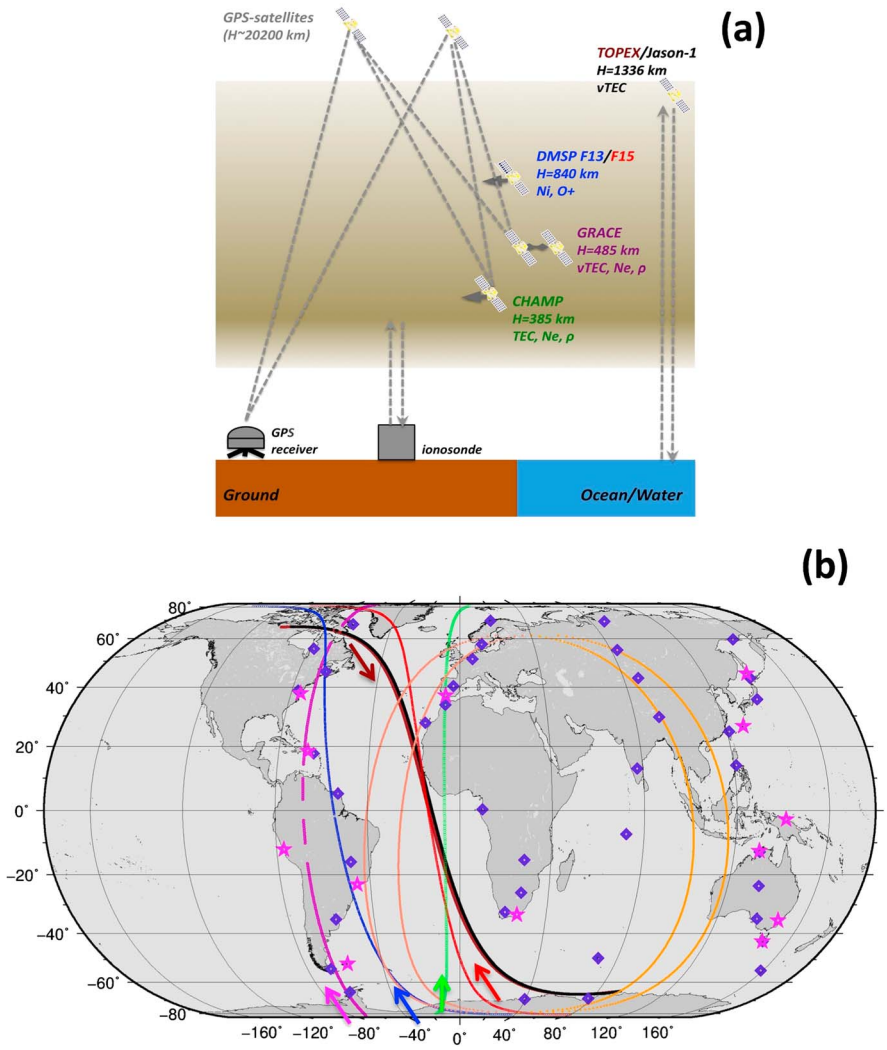

Figure 1. (a) A scheme of an altitudinal distribution and (b) a map with positions of ground-based and spaceborne instruments used in the study. The orbital heights and measured parameters are indicated next to the names of satellites in Figure 1a. The satellites' trajectories at ~21:00–22:00 UT and the position of the solar terminator at altitude 350 km at 21 and 22 UT (the dark orange and orange lines indicate the sunset and sunrise terminators, respectively) are shown in Figure 1b. GPS receivers are marked by violet rhombs and ionosondes by pink stars. The following colors are used throughout the paper to distinguish the satellites' measurements: brown–TOPEX, black–Jason 1, green–CHAMP, blue–DMSP F13, red–DMSP F15, and magenta–GRACE. The arrows show the direction of the satellites' motion.

content (TEC) and further development of the dayside superfountain effect [*Tsurutani et al.*, 2004, 2006, 2007, 2008; *Mannucci et al.*, 2005, 2008, 2009; *Astafyeva*, 2009a, 2009b].

Although prompt penetrating eastward electric fields were proven to be quite important for the development of the dayside superfountain effect, recent modeling studies showed that daytime eastward electric fields on their own are unlikely to produce a large positive ionospheric storm, and the nature of the ionospheric storm depends on the state of the thermosphere. Recent studies suggest that an equatorward neutral wind is required to strengthen the fountain effect and to produce positive ionospheric storms [*Lu et al.*, 2008, 2012; *Balan et al.*, 2009, 2010, 2011]. The mechanical effects of the wind (1) reduce (or stop) the downward diffusion of plasma along the geomagnetic field lines, (2) raise the ionosphere to high altitudes of reduced chemical loss, and hence (3) accumulate the plasma at altitudes near and above the ionospheric peak centered at around ±30° magnetic latitudes [*Balan et al.*, 2010].

Ionospheric effects during numerous geomagnetic storms have now been well documented. A new multi-instrumental era, with a large number of ground-based instruments installed, along with multiple

satellite missions, aids to reveal new aspects of the global development of ionospheric storms with unprecedented detail. However, mostly, ionospheric effects of very intense storms and superstorms have been analyzed, whereas weaker storms should not be neglected as they can also generate very strong ionospheric disturbances. In this paper, we study variations of ionospheric and thermospheric parameters during a moderately intense geomagnetic disturbance of 29–31 August 2004. The use of multiple instruments allows us to (1) have a global overview of the ionospheric storm time behavior during the geomagnetic storm, (2) reveal the regions with largest storm time effects, (3) estimate the contribution of the topside ionosphere in the storm time increase of the ionospheric electron density, and (4) analyze the thermospheric effects during this storm.

2. Data Set

To study ionospheric/thermospheric behavior during the main phase of the storm of 29–31 August 2004, we use a set of the following ground-based and spaceborne instruments (Figures 1a and 1b):

1. Ground-based GPS receivers are a powerful tool for studying the ionosphere. By computing the differential phases of code and carrier phase measurements recorded by the ground-based dual-frequency Global Navigation Satellite Systems (GNSS) receivers, it is possible to calculate the ionospheric TEC along a line of sight between a receiver on the ground and a GPS satellite at an orbital altitude of ~20,200 km. It is generally considered that the TEC is primarily dominated by electron density in the ionospheric *F* region.

   For our analysis, we select several latitudinal (north-south) chains of GPS stations located at different longitudinal sectors. The vertical TEC (vTEC) values were computed from the raw GPS data in receiver-independent exchange format available at the NASA Crustal Dynamics Data Information System archive (ftp://cddis.gsfc.nasa.gov/pub/gps/data/daily/). In order to estimate slant TEC from the frequency-differenced GPS phase delay, the well-known algorithms were used from *Blewitt* [1990] and *Hofmann-Wellenhof* [2001]. The TEC processing algorithm starts with the detection and correction of cycle slips, loss-of-lock and multipath, after which the phase ambiguity is removed, instrumental bias is compensated, and the slant TEC value along the signal path is converted to an effective vTEC. The diurnal vTEC values over the stations were obtained with a 10 min cadence. TEC is measured in TEC units with 1 TECU = 10^{16} el m^{-2}. We assume the accuracy of the vTEC estimations to be of ~1–1.5 TECU.
2. Variations of N_mF_2 and vertical electron density profiles were obtained from ionosondes. Ionosonde measurements are considered as benchmark measurements in the ionosphere's research, since the results depend on electron concentration only and do not contain any instrumental biases. The values of the F_2 layer peak electron density (N_mF_2) were computed at 1 h cadence from hourly f_oF_2 measurements at ionosonde observatories in American and Asian longitudinal sectors. The manually validated f_oF_2 values for the set of the selected ionosondes were obtained from the University of Massachusetts Lowell (UML) Digital Ionogram DataBase (DIDBase) (http://umlcar.uml.edu/DIDBase/), World Data Centre for Solar-Terrestrial Science in Australia (http://www.ips.gov.au/World_Data_Centre/1/3), and the National Institute of Information and Communications Technology (NICT) in Japan (http://wdc.nict.go.jp/IONO/HP2009/ISDJ/index-E.html). In order to retrieve electron density profiles (EDP), the ionograms were manually processed using the ARTIST software [*Reinisch et al.*, 2005].
3. The dual-frequency satellite radar altimeters TOPEX (1992–2006), Jason 1 (2001–2013), and now Jason 2 (from 2008) perform 1 s measurements of vTEC beneath the satellites, i.e., between the water surface and the orbit height of about of 1336 km (http://www.aviso.oceanobs.com/en/missions/index.html). The satellites are in a circular orbit at 1336 km altitude, with an inclination of 66°. They have an orbital period of 112 min and a repeat cycle of 9.9 days. The radar altimeters operate at 5.3 and 13.6 GHz to measure sea surface heights. These measurements are affected by the frequency-dependent retardation/refraction of the radar signal in the ionospheric plasma, and so the dual-frequency measurements can be used to calculate the TEC; the systematic TEC deviation is ~1.5 TECU [*Ping et al.*, 2004; *Yasukevich et al.*, 2009].

   In the current work, we used the data of TOPEX and Jason 1 that are available from the AVISO data center (http://aviso-data-center.cnes.fr/). During the August 2004 storm, the satellites crossed the equator at ~08:56 LT (ascending) and ~20:56 LT (descending).
4. CHAMP (CHAllenging Minisatellite Payload, 2001–2010) was a project of the Potsdam Geophysical Observatory Deutsches GeoForschungsZentrum (GFZ), Germany (http://op.gfz-potsdam.de/champ).

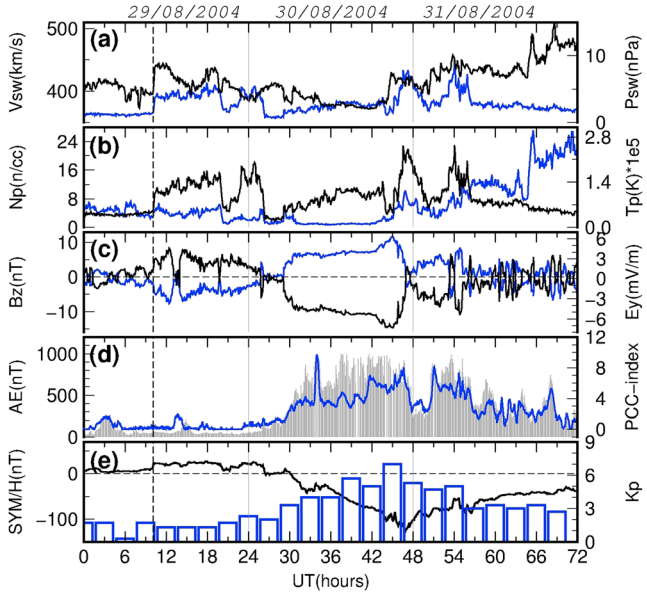

Figure 2. Interplanetary and geomagnetic variations on 29–31 August 2004 (from OMNIWeb Plus services, http://omniweb.gsfc.nasa.gov/). (a) Solar wind speed (black curve) and solar wind ram pressure (blue curve). (b) Proton density (black curve) and proton temperature (blue curve). (c) IMF B_z component (B_z, black curve) and E_y component of the interplanetary electric field (E_y, blue curve). (d) Geomagnetic auroral electrojet index (*AE*, gray bars) and the combined polar cap index PCC (blue curve). (e) Index of geomagnetic activity *SYM-H* (black curve) and planetary index *Kp* (blue bars). All the parameters are 5 min averaged (except for the 3 h index *Kp* and 1 min resolution for the PCC index).

CHAMP had a near-polar near-circular orbit with inclination of 87.3° [*Reigber et al.*, 2002]; its orbital period is about 91 min. The orbit altitude changed from ~450 km in 2001 to ~350 km in 2005; i.e., the satellite passed close to the height of the ionospheric F_2 layer peak density in a meridional direction.

This study used data from three of the instruments on the CHAMP satellite. These are (1) an accelerometer providing data of acceleration due to air drag, which can be further used to calculate the thermosphere neutral density [e.g., *Bruinsma and Biancale*, 2003; *Liu and Lühr*, 2005; *Liu et al.*, 2005; *Doornbos et al.*, 2010]; (2) the Planar Langmuir Probe allowing to determine the in situ plasma density and electron temperature [*McNamara et al.*, 2007]; and (3) a dual-frequency GPS receiver for precise orbit determination (POD) providing TEC measurements between CHAMP and the GPS satellites (20,200 km).

To estimate the vertical TEC from CHAMP's GPS receiver data, we first calculate the slant TEC from pseudorange measurements, as mentioned above. Then, by considering the lower accuracy of absolute TEC with pseudorange observations and the higher accuracy of relative TEC with phase observations, to obtain the absolute slant TEC, we use a phase leveling code algorithm described in *Ma and Maruyama* [2003]. The retrieved slant TEC is further calibrated to remove the instrumental biases. Differential code biases (DCB) for GPS satellites are generated on a daily basis by several centers of the International GNSS Service (IGS) and can be found inside the global ionospheric maps (GIM) TEC product. We use the final IGS GIMs. To estimate the unknown DCB for the CHAMP receiver, we apply the algorithm generally used in University Corporation for Atmospheric Research/Constellation Observing System for Meteorology, Ionosphere, and Climate Data Analysis and Archive Center for low Earth orbit GPS data processing and described in *Yue et al.* [2011]. The slant TEC values were scaled to estimate the vertical POD TEC using a geometric factor derived by assuming the plasma occupies a spherical thin shell at the altitude of 450 km. The elevation angle cutoff was selected as 50°. In the case when several GPS satellites were above the cutoff angle, the values of vertical TEC were averaged to obtain a single POD VTEC value for each epoch.

During the event of 29–31 August 2004, CHAMP flew at a mean altitude of 385 km in the 09:00 LT (descending) and 21:00 LT (ascending) sectors. In addition to the vTEC and the in situ electron density, we also use the CHAMP data of neutral density calculated from the data of the accelerometer onboard the CHAMP satellite, following *Doornbos et al.* [2010]. For the neutral density measurements, the error can reach up to 10–15% during geomagnetic storms and at high latitudes, and it is below 5% during quiet conditions and at low latitudes [*Doornbos et al.*, 2010].

5. GRACE (Gravity Recovery and Climate Experiment) is a satellite mission comprising two identical spacecraft GRACE A and GRACE B, separated horizontally by ~220 km; it was launched on 17 March 2002 into a near-circular, polar orbit (inclination: 89°) with an altitude of about 500 km. Like CHAMP, the GRACE satellites carry accelerometers which provide data of acceleration due to air drag, which has been processed into the data of thermosphere density, and GPS receivers onboard, allowing to calculate the

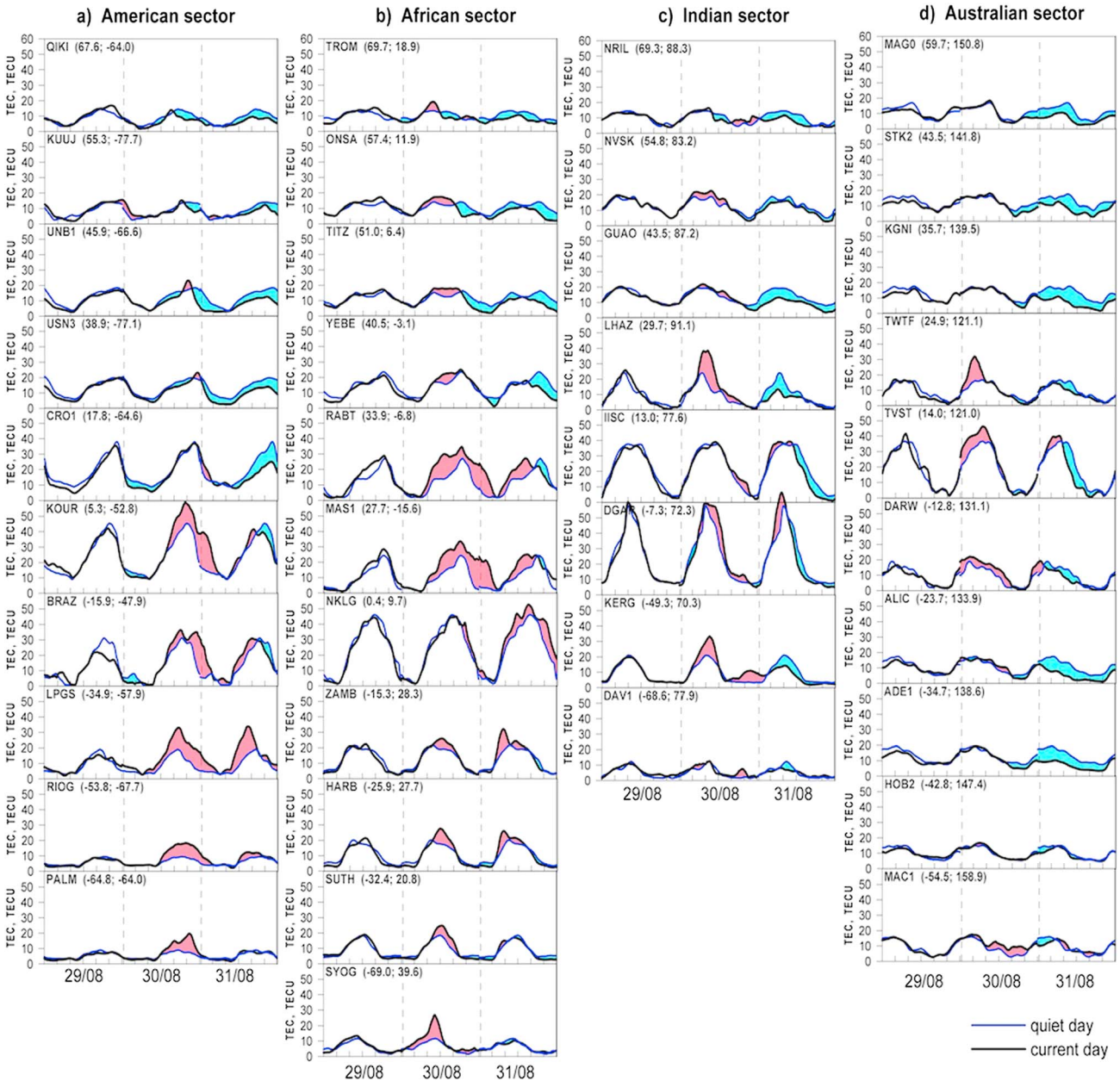

Figure 3. TEC variations as calculated from the data of ground-based GPS receivers located in (a) American, (b) European-African, (c) Asian, and (d) Pacific-Australian longitudinal regions. The names and the geographic coordinates of the GPS receivers are indicated in all panels. The positions of the receivers are shown on the map in Figure 1b. TEC enhancements compared to the quiet day are filled with red, while lower TEC values than on the quiet day are filled with light blue color.

vertical TEC over the satellite using the same method as described above for the CHAMP satellite, but for the ionosphere height of 550 km. In addition, as the spacecraft are interconnected by a K band ranging system using microwave to measure the exact separation distance and its rate of change, we can get the change of the electron density [*Xiong et al.*, 2010].

During the storm, the GRACE satellites were at a mean altitude of 486 km and crossed the equator at about 05:00 LT (descending) and 17:00 LT (ascending).

6. Data of the total ion concentration (Ni in i+/cm3) and of the $O^+/(O^+ + H^+)$ density ratio were obtained with the Special Sensor for ion, Electrons and Scintillation (SSIES) [*Rich and Hairston*, 1994] onboard the Defense Meteorological Satellite Program (DMSP) F13 and F15 spacecraft. DMSP spacecraft are placed in a near circular, Sun synchronous, polar orbit with inclination 98.8° (DMSP F13 platform

document, http://nsidc.org/data/docs/daac/f13_platform.gd.html) and 98.9° (DMSP F15 platform document, http://nsidc.org/data/docs/daac/f15_platform.gd.html). The orbital altitude is ~840–850 km, and the period is ~102 min. The ascending equator crossing time for DMSP F13 is ~18:25 LT and for DMSP F15 satellite is ~21:10 LT.

3. Geomagnetic Storm of 29–31 August 2004

The year 2004 was a year of declining solar activity, with several strong geomagnetic events, including the series of superstorms of 7–11 November 2004 [e.g., *Kelley et al.*, 2003; *Fejer et al.*, 2007; *Mannucci et al.*, 2008, 2009; *Astafyeva*, 2009b; *Lu et al.*, 2012]. One of the most intense storms of 2004, the storm of 24–27 July 2004, provoked a significant long-time positive storm enhancements at low and middle latitudes in the southern hemisphere [*Ngwira et al.*, 2012] and considerably changed the structure of the Earth's radiations belts, both protons and electrons, filling them by fluxes of energetic particles [*Lazutin et al.*, 2008]. These enhanced fluxes remained trapped until the end of August 2004, when a moderately intense storm occurred and caused acceleration and release of the high-energy (>3 MeV) particles [*Lazutin et al.*, 2011, 2012]. In the meantime, the flux of lower energy electrons at the inner shell (L = 2–3) remained highly increased until the November 2004 storm [*Lazutin et al.*, 2012].

Figure 2 shows the variations of interplanetary and geophysical parameters during the storm of 29–31 August 2004. A moderately intense magnetic storm was initiated by the interplanetary shock arrival at ~09:00 UT on 29 August 2004 [*Echer et al.*, 2008]. Considering the time shift of ~64 min due to the solar wind propagation from the registration point by the Advanced Composition Explorer (ACE) spacecraft to Earth, the commencement of the storm can be seen at ~10:04 UT (vertical dashed line in Figure 2) as an abrupt increase of the solar wind speed from 390 km/s to 450 km/s, simultaneously with sudden changes in the solar wind ram pressure and proton density (Figures 2a and 2b). We note that the proton temperature did not change significantly at the shock arrival (blue curve in Figure 2b).

Following the storm commencement at 10:04 UT on 29 August 2004, the initial phase of the storm lasted until ~05:00 UT of the next day, when the IMF B_z turned southward and remained so until ~23:00 UT (Figure 2c, black line). Consequently, the index of geomagnetic activity *SYM-H* started to monotonely decrease until its minimum excursion of −128 nT at 22:50 UT (Figure 2d, black line). The maximum value 7 of the 3-hourly *Kp* index was reached at 21:00 UT on 30 August 2004 (Figure 2d, blue bars). The main peculiarity of this storm is that it was accompanied by sufficiently strong and long-term substorm activity in 30–31 August, as seen from the variations of the auroral electrojet (*AE*) (Figure 2e, gray bars), and which is due to enhanced particle precipitation in the auroral regions [*Lazutin et al.*, 2011, 2012]. Figure 2e also shows the variations of the combined polar cap index (PCC) derived from northern (PCN) and southern (PCS) polar cap indices [following *Troshichev et al.*, 1988, 2006]. Figure 2d indicates on sufficiently strong stress in the tail region and enhanced substorm activity. Release of the stress during this period of time triggered the subsequent decrease of the global ring current and further development of the main phase of the storm. Another increase of the PCC index occurred from ~17:30 UT and lasted until ~23:00 UT (Figure 2d). This period of the enhanced polar cap magnetic activity corresponds to the enhancement in the IMF B_z negative component and to the time of the maximum ionospheric effects observed, as will be shown below.

Overall, this storm was characterized by a very long initial phase (~19 h) and a very long main phase (~17 h). The recovery phase was also very long as it lasted almost 5 days [*Lazutin et al.*, 2011]. Despite being classified as a moderately intense storm, it induced sufficiently strong and interesting effects in the ionosphere; it also caused strong GPS phase fluctuations in the auroral and equatorial regions [*Zakharenkova* and *Astafyeva*, 2015].

4. Results

4.1. Global Ionosphere Behavior During the Main Phase of the Storm of 29–31 August 2004: Ionosphere Variations in the Late Afternoon Sector

To understand the global redistribution of the ionospheric plasma during the main phase of the geomagnetic storm of 29–31 August 2004, we analyze the vertical TEC variations from four latitudinal chains of ground-based

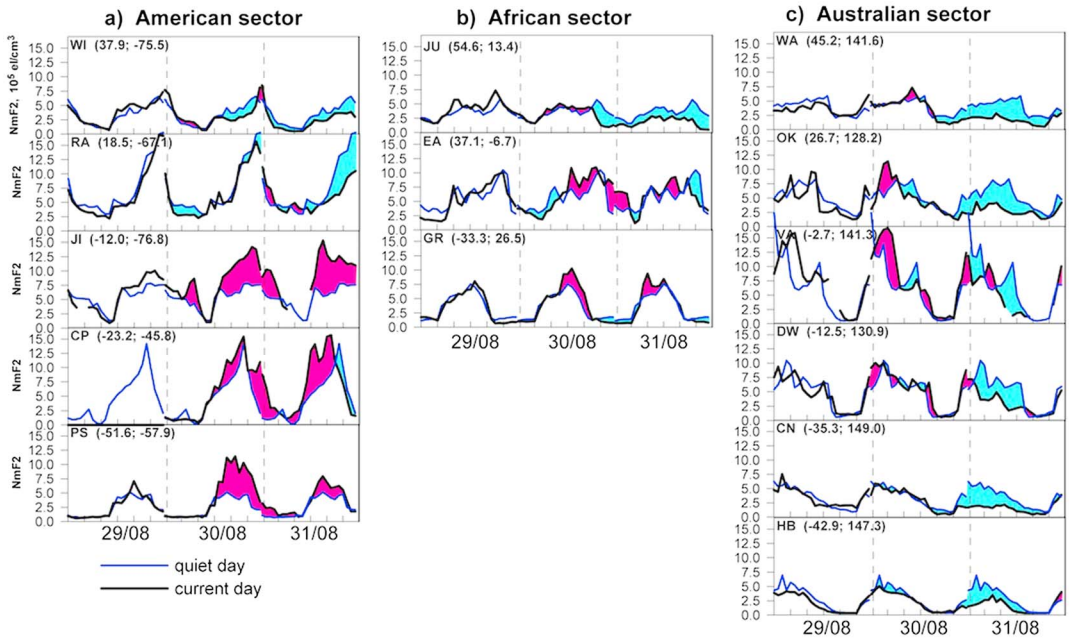

Figure 4. (a–c) Variations of N_mF_2 measured by digisondes in American, European-African, and Pacific-Australian longitudinal sectors, respectively, during the 29–31 August 2004 magnetic storm (black curves) as compared to quiet day 28 August (gray curves). Names of stations and their geographic coordinates are written on the panels. For the CP ionosonde station, no data were available on 29 August, so it was not possible to estimate the storm time changes on that day.

GPS receivers (Figures 1b and 3). We separate the American, African (European), Indian (Asian), and Australian (Pacific) regions (Figures 3a–3d, respectively). Although the coverage was not good everywhere in the world, especially in the southern hemisphere, we managed to have sufficiently even distribution of GPS receivers along the chains (as seen in Figure 1b). To understand the storm time alterations, we compare the storm days 29–31 August with the quiet day of 28 August 2004.

As we showed above, although the SSC time was registered at 10:04 UT on 29 August, the ring current started to slowly intensify only from ~5:30 UT on 30 August and continued to do so until 23:00 UT. One can see that on 29–31 August, the variations in TEC were ambiguous. The first TEC increase of 50–200% occurred from 00:00 to 08:00 UT on 30 August at GPS receivers located at low latitudes in the Australian sector, which corresponded to the morning to noon sectors at that moment (Figure 3d). At the same time, middle- and high-latitude stations showed either a small negative deviation from the quiet time TEC level, or no effect at all. In the Indian sector, a small increase could be seen on 30 August from ~06:00 to 16:00 UT at the low and middle latitudes of the southern hemisphere (Figure 3c). The largest storm time effects in TEC occurred during the main phase of the storm at low latitudes in the African sector (Figure 3b) and from ~14:00 UT in the American sector (Figure 3a). Note that the large TEC increase in the southern hemisphere in both these longitudinal sectors continued until ~06:00–08:00 UT of the next day (Figures 3a and 3b), while in the northern hemisphere, the effects of the storm were much less pronounced.

With the beginning of the recovery phase, on 31 August 2004, large negative effects can be seen in all longitudinal regions, except for the receivers located in the American and African regions of the southern hemisphere, where strong positive alterations were detected (Figures 3a–3d).

Similar effects were observed in data of the ionosondes located in the same longitudinal regions as the GPS receivers (Figure 1b, stars and rhombs). Unfortunately, in the Indian (Asian) region, no digisonde data were available during the time of this storm. We see a primary increase in the dayside values of the N_mF_2 at ionosondes located at low latitudes in the Australian region (Figure 4c). In the European-African sector, the data of three ionosondes showed that the general pattern of N_mF_2 behavior is the same as that for the GPS-TEC (Figure 4b). At the American longitudes, we clearly observed a significant ~100–150% increase in N_mF_2 from ~14:00 UT on 30 August to ~04:00 UT on 31 August; this effect concerned the equatorial station JI

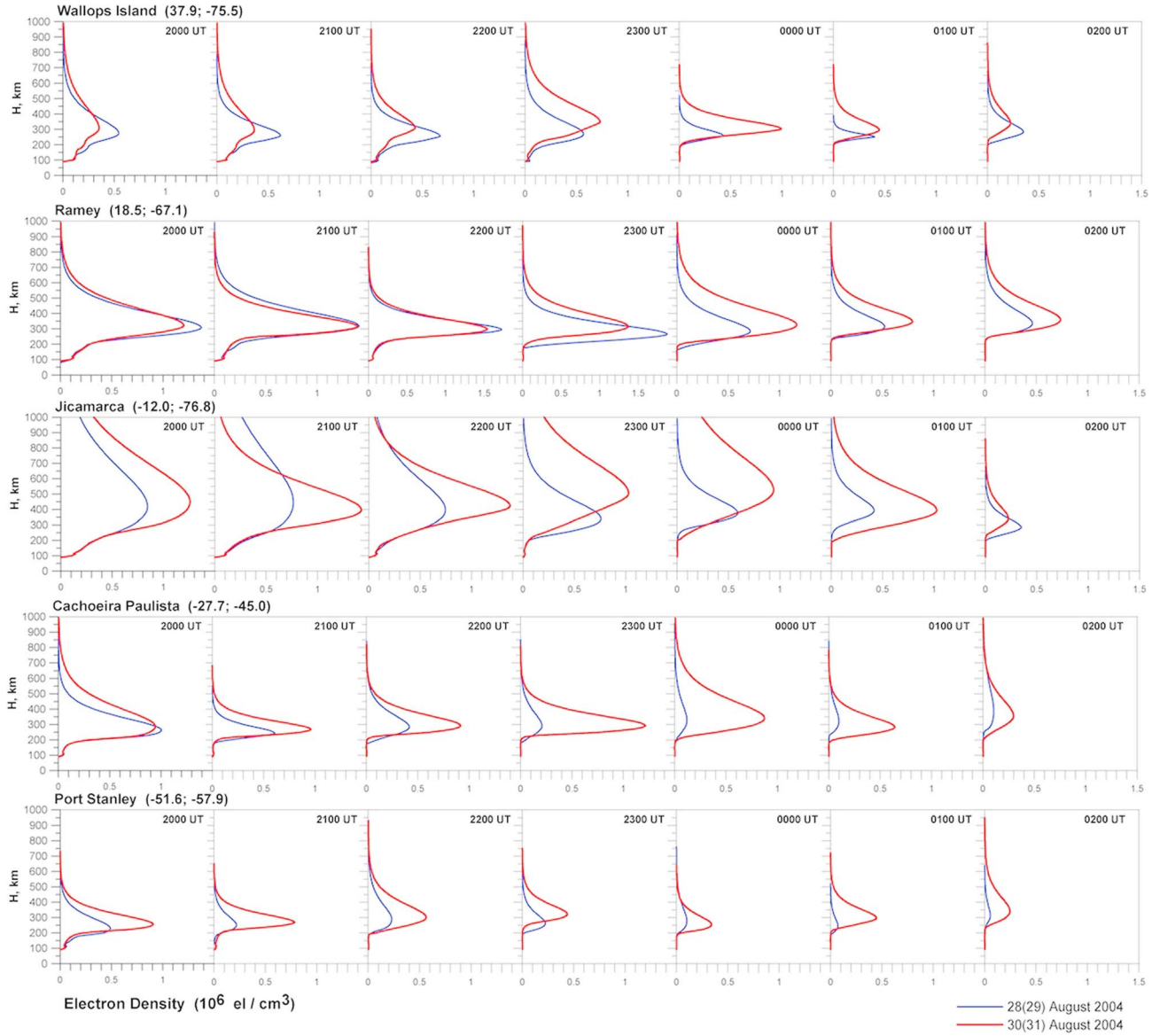

Figure 5. Ionospheric EDP obtained from the data of the digisondes in American region: Wallops Island and Port Stanley (both midlatitude stations), Ramey and Cachoeira Paulista (low-latitude), and Jicamarca (equatorial) stations. The time period concerned is from 20:00 UT on 30 August to 02:00 UT on 31 August 2004.

and the other two ionosondes located in the southern hemisphere (Figure 4a). Whereas, at the midlatitudes of the northern hemisphere, we observe the development of the negative storm from ~13:00 to 15:00 UT on 30 August. We note that this negative storm effect in the northern hemisphere (NH) is somewhat less evident from the TEC data as shown in Figure 3, while the strong positive storm in southern hemisphere (SH) is seen in both the TEC and N_mF_2 observations. From these simultaneous observations, we can conclude that the observed positive storm in SH occurred in the ionospheric *F* layer, whereas the observations in NH may indicate on somewhat opposite effects in the ionospheric response above the ionospheric *F* layer, i.e., in the topside ionosphere.

Indeed, in the data of the vTEC above the height of the GRACE satellite of 485 km (~17:00 LT sector), signatures of the positive ionospheric storm at low latitudes were observed (Figures 5 and 6, second column). The equatorial and low-latitude TEC 1.5–2 times exceeded the quiet time levels. This increase started about 4 h after the beginning of the main phase of the storm and continued until the next day, gradually decreasing with time. In addition to that, we also notice a small TEC increase at midlatitudes of the NH starting from

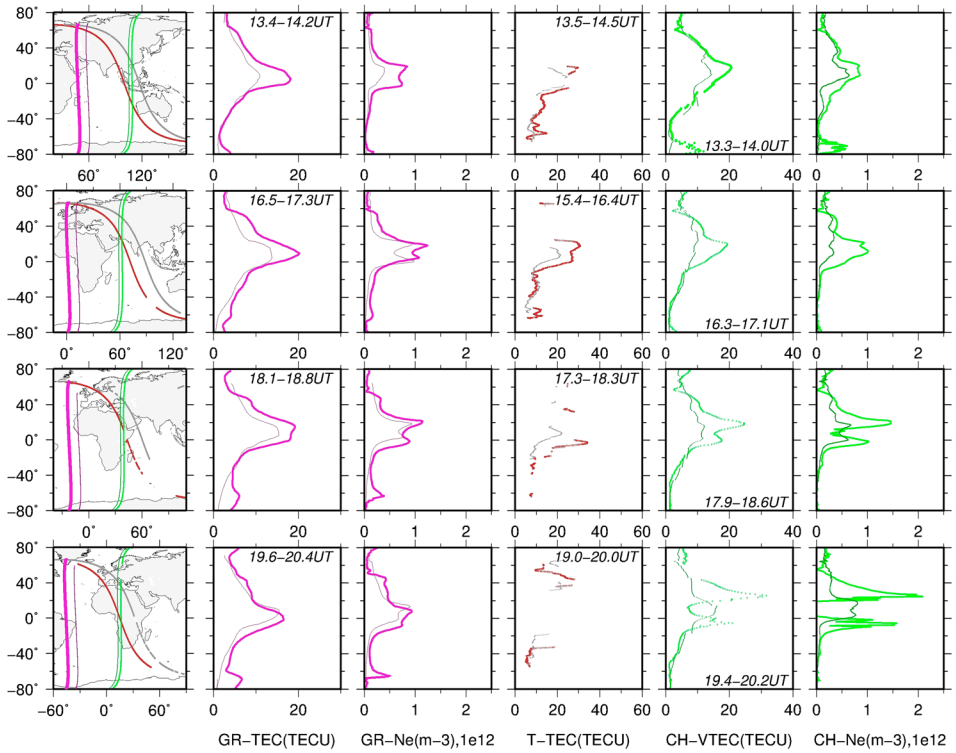

Figure 6. Ionospheric behavior in the afternoon and the postsunset sector during the main phase of the geomagnetic storm on 30 August 2004. Vertical TEC (GRACE– magenta curves, TOPEX–brown curves, and CHAMP–green curves) and electron density observations (GRACE and CHAMP) are compared with the quiet day 28 August (gray, dark gray, and dark green curves, respectively). (first column) The trajectories for all the satellites are shown. GRACE crosses the equator at ~17:00 LT, TOPEX at 20:56 LT, and CHAMP at ~21:00 LT.

~13:00 UT. This vTEC increase in the NH lasted until the beginning of the recovery phase of the storm. From 18:00 UT, we observe a growth of TEC in the high latitudes of the SH and from 22:00 UT, a growth of TEC in the midlatitudes of the SH. Similar behavior can be concluded from the variations of the electron density Ne at the orbital height of the GRACE satellite (Figure 6, third column). One can see a small storm time enhancement of the Ne throughout the main phase of the storm, and we also observe two-peak structure of the equatorial ionization anomaly (EIA). Starting from ~17:00 UT, we notice hemispheric asymmetry, when the northern EIA crest showed a larger peak of density, and an increase of Ne can be seen at high and middle latitudes of the NH. Development and traveling of high-latitude traveling ionospheric disturbances (TID) is also clear from the panels (Figures 5 and 6).

To have a better overview on the ionospheric latitudinal redistribution during the maximum of the ionospheric disturbance, here we analyze the EDP from the ground-based digisondes located in the American sector (Figure 1b). The distinguished feature of the EDP's behavior on the disturbed day is a significant uplift of the F_2 layer peak (Figure 5). Besides, we can clearly see the seasonal effect with the dominance of a negative phase of the ionospheric storm in the NH (summer) and the pronounced positive phase in the SH (winter). At the northernmost station (Wallops Island), we notice a negative ionospheric storm during local evening time, followed by a short-time positive storm (23:00–01:00 UT); this effect is also recognized in the GPS TEC data (Figure 3). Similar behavior was observed at 00:00–02:00 UT for the ionosonde Ramey and CRO1 GPS stations. For these moment, the height of F_2 layer peak increased, which that can be associated with an up-flow of the ionospheric plasma along magnetic field lines. At the middle latitudes of the southern hemisphere (Cahoeira Paulista and Port Stanley), a significant 200–300% enhancement of the electron density was registered. The enhancement can be caused by the plasma fluxes from the plasmasphere and the F_2 layer uplift due to vertical drift. It is interesting to note the storm time effects on Jicamarca station located on geomagnetic equator, where the strong enhancement of electron density of F_2 layer was detected simultaneously with the layer uplifting up to 500 km; this can be explained in terms of storm time changes of $E \times B$ plasma drifts.

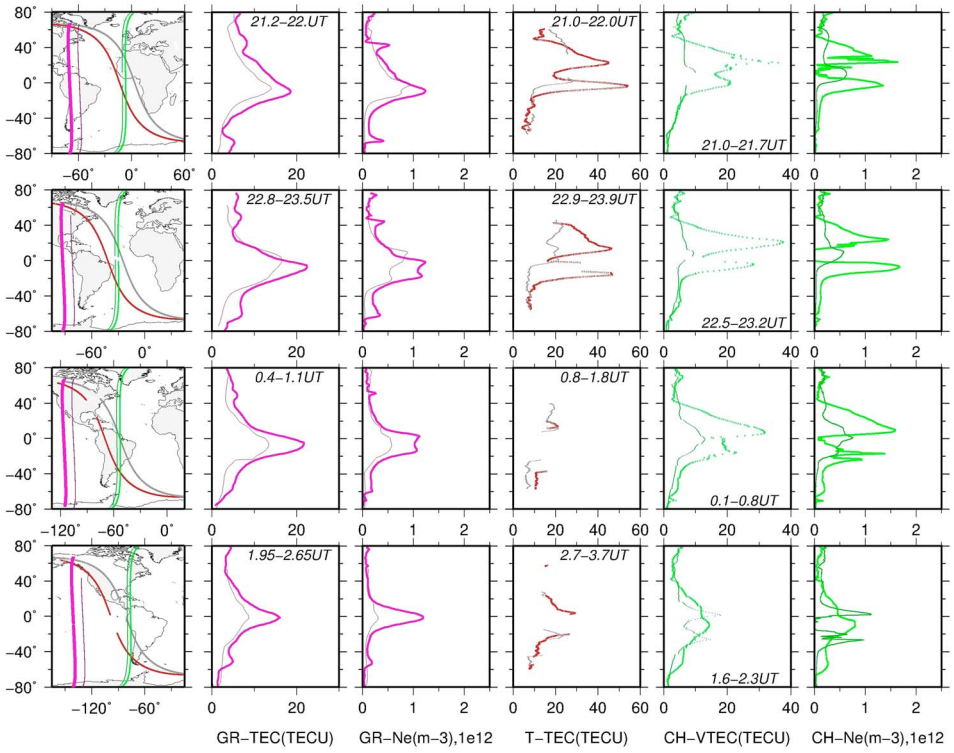

Figure 7. Same as Figure 6 but for the time period from 22:00 UT on 30 August to 03:00 UT on 31 August 2004.

Thus, ground-based TEC-measurements and the ionosonde stations clearly show the dayside low-latitude enhancement of the ionospheric TEC and plasma density in all the longitudinal sectors during the main phase of the storm. The GRACE observations confirm the occurrence of the positive storm at low latitudes but, at the same time, reveal a north-south asymmetry in the ionospheric behavior at middle and high latitudes. Taking into account that GRACE passes in the topside region, we can conclude the opposite asymmetries in the *F* layer and the topside region. The largest storm time effects were observed in the southern hemisphere in the African and American sectors from ~13:00 UT on 30 August to 04:00–06:00 UT on 31 August, which correspond to the afternoon and postsunset local sectors. The latter region is of great interest because the physical mechanisms are different from those that produce effects in the dayside afternoon region and are less understood. We discuss them below.

4.2. Ionospheric Storm Time Effects in the Postsunset Sector

To analyze in more detail the storm time ionospheric effects in the postsunset sector, here we use the data of multiple satellites that during the storm crossed the equator at ~20:35–21:10 LT (Figures 1a and 1b). Such a unique configuration of satellites provides us with a very interesting set of data, allowing us to obtain altitudinal distribution of the storm time effects in the ionospheric plasma.

Figures 6 and 7 show the measurements of vertical TEC as deduced from satellite radar altimeter TOPEX (Figures 6 and 7, fourth column, brown curves), as well as from GPS onboard the CHAMP satellite, and in situ measurements of electron density performed by CHAMP (Figures 6 and 7, sixth column, green curves). The results of the Jason 1 are quite similar to those by TOPEX, so we do not show them in the paper. Here we analyze the TEC alterations from ~13:30 UT on 30 August to ~ 3:00 UT on 31 August 2004, and we also compare the storm time values with a geomagnetically quiet day 28 August 2004.

Similar to the ground-based GPS receivers (Figure 3), satellite observations show 70–100% enhancement during the main phase of the storm in the equatorial and low-latitude TEC and electron density as compared to the quiet day (Figure 6). This effect can be seen in all satellite data from 13:30 UT to 16:00 UT. We also observe a north-south asymmetry in the latitudinal profiles from CHAMP. We note that during this period of time, GRACE, which passed in the ~17:00 LT region at ~485 km, showed very similar behavior, and the values

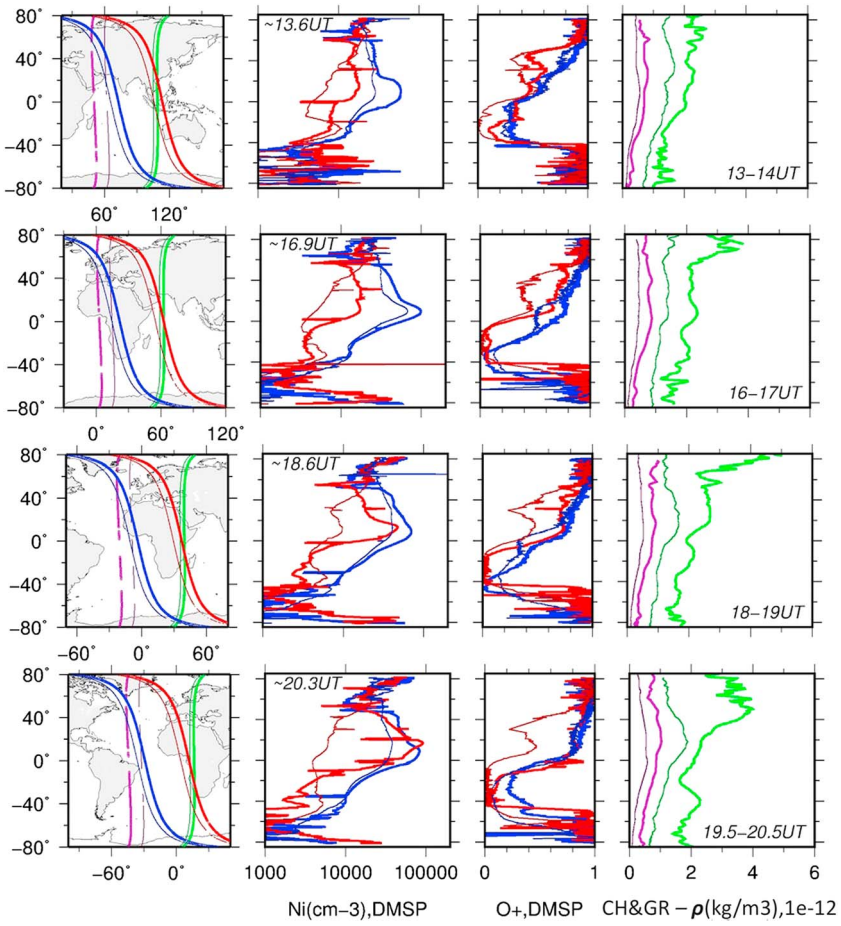

Figure 8. (second and third columns) Ion density (Ni) and O+ ratio as measured by DMSP F13 (blue) and F15 (red) spacecraft from 13:00 to 21:00 UT on 30 August 2004. The storm time values are compared to the quiet time ones (dark blue for F13 and dark red for F15). (fourth column) Neutral mass densities (ρ) measured by the CHAMP (green) and GRACE (magenta) satellites at the main phase of the storm and during the quiet time (dark green and dark magenta, respectively). (first column) The corresponding trajectories for all the satellites are shown. DMSP F13 crosses the equator at 18:30 LT and F15 at 21:10 LT; CHAMP and GRACE satellites do that at ~21:00 LT and ~17:00 LT, respectively.

of the vTEC were close. From ~17:30 UT, when the IMF B_z dropped further southward, and the polar cap magnetic activity increased (Figure 2), the CHAMP GPS measurements revealed further increase of the low-latitude vTEC, with concurrent appearance of the two-crests structure of the EIA. During that time, the TEC in the northern crest of the EIA was ~08:00–09:00 TECU higher than that in the southern one. The CHAMP in situ measurements revealed even stronger storm time development of the EIA with larger difference between the crest and trough electron densities, and they also confirmed the asymmetry between the northern and southern crests. Unfortunately, data of the satellite radar altimeters contained large gaps due to the spacecraft passing over land, so it was difficult to compare the measurements at different heights for that period of time.

The strongest storm time effects were observed from ~19:00 to 24:00 UT, when all signatures of the occurrence of the superfountain effect (SFE) were seen in both vertical TEC and electron density. The crests of the EIA shifted poleward to ±20° of latitude, as the altimeter data show in Figures 6 and 7. The TEC at the crests reached 50–55 TECU for both TOPEX and Jason 1 measurements, while the TEC at the trough concurrently decreased to 15–20 TECU. Simultaneously, the TEC above CHAMP increased up to 35–40 TECU. Knowing that these two spacecraft passed in practically the same longitudinal sector but at different altitudes (Figures 1a and 1b and Figures 6 and 7), we estimate the ratio of the bottomside/topside contribution. Considering the topside vTEC over the TOPEX satellite as 2–3 TECU [*Yizengaw et al.*, 2008], we estimate the ratio as about 3:7, which implies significant ionospheric uplift over the height of the ionospheric *F* layer.

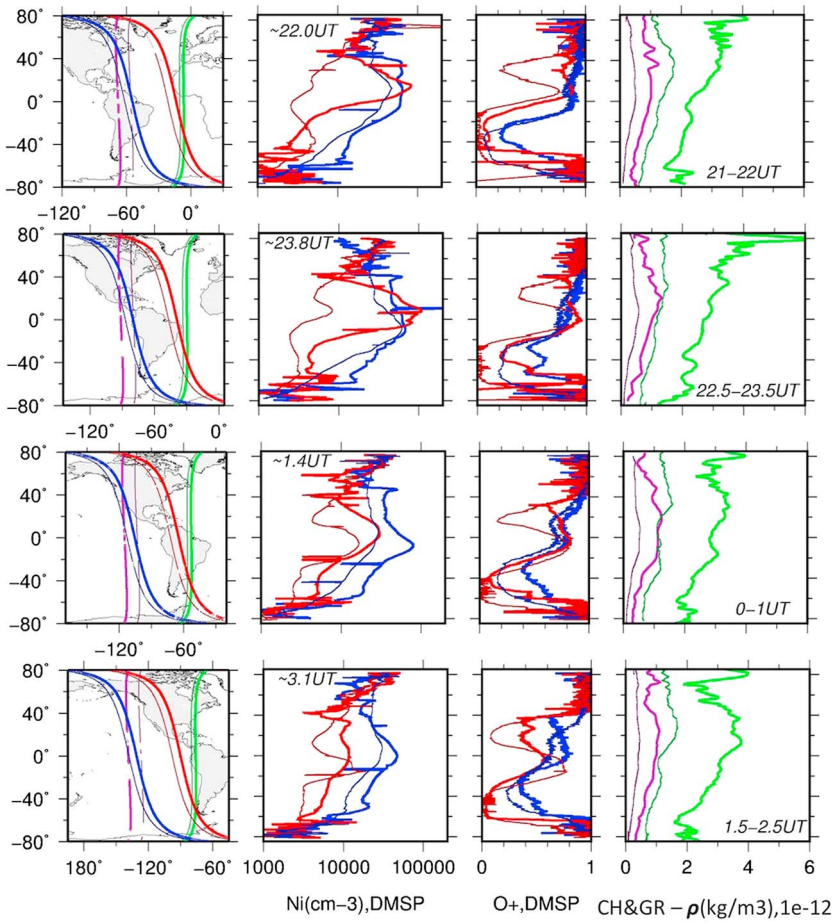

Figure 9. Same as in Figure 8 but for DMSP observations from 22:05 UT on 30 August 2004 until 04:08 UT 31 August 2004 and for CHAMP and GRACE observations from 21:00 UT on 30 August 2004 to 03:00 UT on 31 August 2004.

Indeed, the TEC above CHAMP increased ~3.5–4 times as compared to the quiet time levels. TOPEX and Jason 1 observations confirm the overall increase of TEC below 1336 km. The CHAMP in situ measurements of the electron density Ne also revealed a significant storm time increase over the EIA crests with a simultaneous drop over the magnetic equator (Figures 6 and 7, sixth column).

Besides sufficiently large contribution of the topside ionosphere during this storm, our observations signify an ionospheric uplift to high altitudes. To further check the altitudinal extent of the storm time ionospheric effect, here we analyze data of the ion density at the height of ~840 km as measured by the DMSP F13 and F15 spacecraft. Note that the DMSP F15 satellite passed at ~21:10 LT, i.e., in the postsunset sector, and the F13 crossed the equator at ~18:30 LT, i.e., in the late afternoon-evening sector (Figure 8). Similar to the TEC and Ne measurements, the Ni values from both spacecraft (F13 and F15) exceeded the quiet time level at the equator with the development of the main phase of the storm (as shown on the example of 13:00 UT in Figure 8). One can see that before ~19:00 UT, the ion density at the postsunset sector (from F15, red curves) was about 10 times less than that in the evening sector (from F13, blue curves). Starting from ~19:00 UT, the ion density at the magnetic equator and nearby started to largely increase, and by 21:00–22:05 UT, it exceeded almost 100 times the quiet time level and reached the level of the evening-sector ion density (Figure 8). At 22:00–24:00 UT, the Ni in the postsunset sector slightly exceeded the storm time Ni value in the evening sector (Figure 9, first and second columns). The ion uplift signatures started to diminish from ~01:00 UT in 31 August as seen from all satellite measurements, including DMSP. By 03:00 UT on 31 August 2004, the TEC, Ne, and Ni values come back to nondisturbed (Figures 7 and 9, the bottom line of each panels).

Besides the low-latitude Ni uplift until 840 km, from 17:00 UT on 30 August 2004, we observed Ni increase at middle and high latitudes of the northern hemisphere, while in the southern hemisphere, the storm time levels hardly exceeded the quiet time ones. The Ni uplift finally extended to the southern hemisphere from 23:05 UT and lasts only 1.5 h before going down to the undisturbed level. This storm time hemispheric asymmetry can also be clearly seen in the data of $O^+/(O^+ + H^+)$ postsunset density ratio as measured by the DMSP F15 satellite (Figures 8 and 9, third column); one can see that in northern hemisphere, before 20:00 UT O^+ ions constituted ~80% of ions detected, whereas from 20:05 to 24:00 UT, the number of O^+ ions increased over all latitudes of northern hemisphere, including the equatorial region. At the same time, in the southern hemisphere, the O^+ density ratio reached about 20% at middle latitudes and 50–90% at high latitudes at ~22:00 UT. We note that the effect of oxygen ions uplift to DMSP satellite has already been reported for several ionospheric superstorms and is considered as a signature of prompt penetration of intense dawn-to-dusk interplanetary electric fields and further development of the dayside SFE [*Tsurutani et al.*, 2006, 2007]. Our observations indicate a stronger ionospheric uplift in the NH than in the SH.

Finally, we notice rapid fluctuations of the electron (at 400 km) and ion density (at 840 km) in both CHAMP and DMSP measurements from 19:00 UT on 30 August to ~02:00 UT on 31 August, which indicates the presence of plasma bubbles at low latitudes in the postsunset region and at high latitudes (as discussed in detail by Zakharenkova and Astafyeva (2015)).

4.3. Thermospheric Behavior in the Late Afternoon and Postsunset Sectors

The variations of the neutral mass density ρ (thermospheric storm) during the main phase of 29–31 August 2004 geomagnetic storm are shown in Figures 8 and 9 (fourth column). The neutral density data were derived from the CHAMP (~21:00 LT, ~385 km) and GRACE (~17:00 LT, ~485 km) satellites. In both longitudinal sectors, ρ started to gradually increase shortly after the beginning of the main phase of the storm at ~10:00 UT and reached their maximums by 23:00–24:00 UT of 30 August. However, in the evening of the ~17:00 LT longitudinal region, the storm time effects were much less pronounced than in the postsunset ~21:00 LT region. Such a difference is, most likely, due to different local time sector for these two satellites.

In the ~17:00 LT afternoon region, a small growth of the neutral density at ~485 km (magenta curves) was observed throughout all the latitudes; it increased gradually with the development of the main phase of the storm. No clear hemispheric asymmetry was observed in the data of neutral density at this height and this local region. However, we notice the occurrence of large-amplitude TAD structure at ~22:00 UT at high latitudes in the northern hemisphere. We suggest that this TAD caused an increase of ρ over low latitudes about 90 min after. By 00:00–01:00 UT, the density reached its maximum value of $\sim 1.2 * 10^{-12}$ kg/m^3 over low and midlatitude regions. The thermospheric storm continued all day on 31 August 2004 and gradually quieted on 1–2 September 2004 (not shown here).

In the postsunset sector, CHAMP showed a significant increase in the neutral mass density at 385 km as compared to the quiet time level and as compared to the late afternoon region (green curves in Figures 8 and 9). Moreover, from 16:00 UT, we see a very large thermospheric disturbance developing over the northern polar region; the disturbance descends toward the high and midlatitudes within the next 2 h, causing an overall increase of the neutral density in the northern hemisphere. At the same time, a smaller ρ enhancement can be seen in the high-latitude region of the southern hemisphere. The maximum perturbation was reached by 22:00–23:00 UT, when the density over the north polar cap and high-latitude region reached ~4 times the quiet time level and an overall 200% increase was observed over other latitudes. Similar to the late afternoon sector, the neutral density remained largely increased during the next few days of the recovery phase of the storm.

Overall, the development of the 30–31 August thermospheric storm seemed to similarly occur during other storms [e.g., *Balan et al.*, 2011, 2012]. The neutral density increased at high latitudes shortly after the onset of the main phase and several hours later the enhanced ρ reached middle and low latitudes. The high-latitude density increase was especially strong in the northern hemisphere in the postsunset region, as shown by the CHAMP measurements. This hemispheric difference can be explained by the seasonal effect, i.e., by the northern polar cap and auroral region (local summer) being constantly heated, while most of the southern polar region was in the shadow. Although that it was believed that lower solar heating in winter hemisphere would provoke larger storm time disturbances, recent observations showed the opposite effect, as demonstrated in previous observations by CHAMP during three superstorms [*Liu and Lühr*, 2005] and in the current manuscript.

5. Discussions and Conclusions

The use of multiple ground-based and spaceborne instruments allowed us to analyze in detail the ionospheric and thermospheric response to the moderately intense geomagnetic storm of 29–31 August 2004. Overall, we observe a very complex behavior of the ionospheric storm development:

1. A positive storm in TEC and N_mF_2 started to develop at low latitudes with the beginning of the main phase and persisted until the recovery phase. The large dayside low-latitude enhancement was also seen in the topside ionosphere, as shown by the GRACE and CHAMP satellites, and reached as high as 840 km of altitude, as seen in the data of the DMSP F13 and F15 satellites.
2. Data of ground-based GPS receivers and ionosondes revealed a strong positive storm in the ionospheric *F* layer in the SH in the American and European-African sectors; at the same time, in the data from the NH, we observed no or a very small and short-term positive effect, followed by larger negative deviations during the main phase of the storm.
3. The satellites' data covered the topside region and detected opposite asymmetry than was observed in the *F* layer, i.e., larger TEC and Ne values in the NH, and no or small storm time enhancement in the SH. This phenomenon was observed in both late afternoon (17:00–18:00 LT) and postsunset (~20:30–21:30 LT) sectors, and it was also shown to reach at least 840 km of height.
4. The hemispheric asymmetry can also be seen in the data of the neutral density but only in the postsunset region (CHAMP measurements at 385 km altitude), while in the evening sector, GRACE data showed rather "even" increase throughout all the latitudes with no asymmetry (at 485 km). Overall, the thermospheric storm in the postsunset sector was found to be much stronger than in the evening sector.
5. In the postsunset sector, we observed a strong storm time reinforcement of the EIA, also known as a superfountain effect. At the end of the main phase of the storm, about an hour after a further intensification of the IMF B_z component, TEC and Ne within the crests of the postsunset EIA increased up to 250%; this effect further strengthened during the next 4–5 h and lasted until the beginning of the recovery phase. The contribution of the topside ionosphere was estimated to be significant (about 3:7). DMSP observations showed a rise of the ionospheric plasma to at least 840 km, and simultaneously the O^+ ratio density increased in the equatorial region and in the northern hemisphere, also indicating the hemispheric asymmetry.

The observed opposite interhemispheric asymmetry in the ionospheric storm time behavior at different heights is a very interesting feature of the considered ionospheric storm and seems to be observed for the first time. The north-south asymmetry in the ionospheric response in the *F* region has been already reported during a number of geomagnetic storms [e.g., *Karpachev et al.*, 2007; *Astafyeva*, 2009b; *de Abreu et al.*, 2010; *Ngwira et al.*, 2012; *Zakharenkova et al.*, 2014]; it is usually attributed to seasonal effects, as it is known that the positive phase often occurs in the winter hemisphere, while negative storm is more summer hemisphere "feature" [e.g., *Prölls*, 1995; *Goncharenko et al.*, 2007; *Danilov*, 2013]. The difference in the ionospheric response in the *F* layer and in the topside ionosphere has already been observed during the superstorm of 20 November 2003 [*Yizengaw et al.*, 2006]. The authors reported that the topside ionosphere and plasmasphere did not show significant storm time alterations, while data of ground-based GPS receivers indicated a large dayside enhancement. Later, *Pedatella et al.* [2009] on the example of the geomagnetic storm of 15 December 2006 demonstrated a significant enhancement of the topside/plasmasphere TEC above ~550 km, while these effects were much less pronounced in measurements of satellite altimeters TOPEX/Jason 1. Their observations suggested that the topside TEC increase was caused by soft particle precipitation. In our case, we observe opposite asymmetries in the *F* layer and in the topside ionosphere/plasmasphere, which clearly implies different drivers for these two altitudinal regions. The low-latitude and SH positive storms in the *F* layer (increases in N_mF_2 and TEC) are usually attributed to either a downwelling of neutral atomic oxygen as a result of the storm time induced thermospheric circulation, or to uplifting of the F_2 layer because of the vertical drift [*Buonsanto*, 1999; *Danilov*, 2013]. In addition, plasma fluxes from plasmasphere can also make a possible cause of the positive ionospheric storm in the *F* layer. The NH positive storm in the topside ionosphere seemed to respond to storm time alterations in the neutral density that were much stronger over the northern polar and the NH high-latitude regions.

Another interesting feature of the 29–31 August 2004 storm is the observation of the SFE in the postsunset region (~20:30–21:30 LT). The dayside SFE is a well-known and well-described phenomenon [e.g., *Kelley*, 2009;

Mannucci et al., 2005; *Tsurutani et al.*, 2004, 2006], that is primarily driven by unshielded prompt penetration of interplanetary and polar cap electric fields to the equatorial and near-equatorial ionosphere. The presence of the storm time enhanced electric fields implies enhanced $E \times B$ upward convection of the equatorial and near-equatorial plasma, which can reach as high as 800–1000 km of altitude. Once the dayside ionospheric plasma is uplifted, the recombination rate of this plasma is reduced [e.g., *Tsurutani et al.*, 2006 At the same time, solar photoionization regenerates a new ionosphere at lower altitudes leading to overall TEC enhancement in the equatorial and low-latitude region. Furthermore, the plasma transported to higher altitudes is moved to higher magnetic latitudes assisted by the gravitational force [*Richmond and Lu*, 2000; *Kelley et al.*, 2004, 2009; *Tsurutani et al.*, 2004, 2006]. However, this explanation is valid to explain the dayside SFE, whereas in the night, dawn and dusk regions there may be other drivers or their combination. The latter becomes a very important question in the framework of the current study, as we observe sufficiently strong signatures of the SFE in the postsunset sector, i.e., in absence of direct ionization by the solar irradiance.

It is known that even under quiet conditions, the equatorial fountain effect is often most pronounced near the dusk region, where there exists a large eastward electric field associated with the "prereversal enhancement" of the zonal electric field [*Woodman*, 1970; *Sastri*, 1982; *Kelley et al.*, 2009; *Lu et al.*, 2012]. This phenomenon causes a brief and intense uplift of the electric field near sunset, which results in a height increase in the equatorial ionosphere and in an overall enhancement of the EIA. The latter is driven by an apparent renewal of the fountain effect due to an increase of the eastward electric field, which, in turn, causes an increased outflow of ionization from the through region, thereby increasing the ionization density at the crests at the expense of that at the through, thus enhancing the crest-to-trough density ratio of the EIA [e.g., *Sastri*, 1982].

During geomagnetic disturbances, in the dusk sector, the eastward penetration electric field, associated with the negative IMF B_z, adds to the postsunset eastward electric field because of the *F* region dynamo [e.g., *Blanc and Richmond*, 1980; *Basu et al.*, 2007] and to overshielding due to region 2 field-aligned currents (FACs) [*Kikuchi et al.*, 2008]. Here we observe significant reinforcement of the EIA near ~21:00 LT sector, so that the main questions are: how far from the dusk region can the effects of the prereversal enhancement last? And, in the absence of the solar ionization, what are the mechanisms responsible for the development of the EIA and the SFE in the postsunset sector? Modeling studies suggest that during the main phase of a geomagnetic storm and in the presence of FACs, the dayside eastward electric field is extended from before the sunrise morning sector (~06:00 LT) to the postsunset region, merely until the ~22:00 LT sector [*Tsunomura*, 1999; *Kikuchi et al.*, 2008]. In the case of the 29–31 August 2004 storm, we did not observe any signatures of the EIA enhancement at ~08:00–09:00 LT (not shown here). In the postsunset region, our observations of the SFE signatures are in agreement with the modeling, as the extension of the dayside electric fields until ~22:00 LT can explain the observed poleward displacements of the EIA crests observed from 17:00 UT (30 August) to 02:00 UT (31 August), as well as the ionospheric uplift to at least ~840 km altitude; however, analyzing the storm time behavior of the ionospheric parameters (Figures 6 and 7), it is difficult to attribute the observed TEC and Ne increase solely to the storm time increased electric fields and further EIA redistribution, as there seem to act an additional source of the plasma ionization, which, eventually, led to such high values of plasma density in the EIA crests.

The ionospheric plasma is created as the neutral constituents are ionized by sunlight and by precipitating energetic auroral particles, and it is destroyed by chemical reactions that eventually lead to recombination of the ions and free electrons at the height of the ionospheric *F* region. In our case, the low-latitude part and the entire southern hemisphere part of the satellites tracks lied in the unlit area (Figure 1b), so that the measurements were done ~2 h after the sunset line at ~350 km. Therefore, the observed enhancement in the electron density was, most likely, caused by other source than the solar irradiance. We consider that in addition to the storm time eastward prereversal enhancement, the storm time increased thermospheric density could produce that effect on the ionosphere, as we observed significant increase of the neutral density in this sector and equatorward propagation of TADs and TIDs from high-latitude regions.

The largest storm time ionospheric and thermospheric alterations started around 17:30 UT, when the IMF B_z intensified and when the magnetic activity in polar regions increased. Then, according to the assimilative mapping of ionospheric electrodynamics services (AMIE2) [*Richmond and Kamide*, 1988]; available from http://spidr.ngdc.noaa.gov), this period of time was characterized by a sudden strong increase in the

simple Joule heating and cross polar cap potential; these variations were slightly more intensive in the northern hemisphere. It is known that during geomagnetic storms, the enhanced Joule heating over high latitudes lifts the neutrals and drives them toward the low and equatorial latitudes, thereby changing thermospheric composition globally [e.g., *Fuller-Rowell et al.*, 1994, 2008]. This storm-induced circulation augments the normal seasonal circulation from summer to winter. As a result, in the NH, the perturbations can be easier transported to middle and low latitudes than in the SH. Knowing that the equatorward expansion of the thermospheric neutral composition disturbance preferentially occurs in the midnight-postmidnight sector during the main phase of storms owing to the reduced ion drag and equatorward background wind in this sector [*Prölls*, 1995; *Danilov*, 2013], this could explain our observations of much stronger thermospheric effects in the northern high latitudes in the postsunset region, and a strong TAD traveling from the northern high latitudes in the evening sector. Our observations of gradual uplift of O^+ in the northern hemisphere can confirm the role of the thermosphere in the ionospheric uplift and the development of the SFE in the postsunset sector. Our results are also in agreement with the recent observations of strong termospheric effects by CHAMP for three superstorms of 2003–2004 [*Liu and Lühr*, 2005].

The recovery phase of the 29–31 August 2004 storm lasted 5 days [*Lazutin et al.*, 2011]. The beginning of the recovery phase, on 31 August, was accompanied by a sufficiently large negative storm in all longitudinal sectors of the northern hemisphere (Figures 3 and 4); in Australian and Indian sectors, the negative storm was observed at all latitudes. Whereas, in European-African and American sectors a positive storm seemed to continue. The negative ionospheric storms are generally believed to be caused by the changes in the thermospheric composition because of the heating of the thermosphere during geomagnetic disturbances [*Prölls*, 1995; *Fuller-Rowell*, 2011; *Danilov*, 2013]. The storm time equatorward neutral wind makes the thermosphere richer in molecular [N] concentration and poorer in atomic [O] concentration so that chemical recombination becomes faster than normal [e.g., *Fuller-Rowell et al.*, 1994, 2008]. Indeed, according to our results, the increase of the thermospheric neutral density accompanied the negative ionospheric storm on 31 August 2004, when the recovery began. The occurrence of positive storm in the SH at the recovery phase is also in agreement with previous observations, showing that in winter, positive phases are more probable [*Goncharenko et al.*, 2007; *Danilov*, 2013].

Thus, our study proves again that weaker geomagnetic storms are not to be disregarded. The storm of 29–31 August 2004 had a minimum *Dst* excursion of "only" −128 nT and passed unnoticed by the community; however, it provoked quite significant ionospheric and thermospheric disturbances, especially in the postsunset sector. Multi-instrumental studies can be very effective in understanding of storm time ionospheric redistribution, and future works and new satellite missions will undoubtedly shed more light on such a complex subject as ionospheric storms.

Acknowledgments

This work is supported by the European Research Council under the European Union's Seventh Framework Program (ERC grant agreement 307998). We acknowledge the use of NASA/GSFC's Space Physics Data Facility's OMNIWeb (or CDAWeb or ftp) service, and OMNI data for the data of interplanetary and geophysical parameters, and pc-index.org services for the data of polar cap magnetic indices PCN and PCS. We thank the AVISO data center (http://aviso-data-center.cnes.fr/) for the data of satellite altimeters TOPEX and Jason 1 and GFZ Potsdam for providing the data of CHAMP satellite through the ISDC data center. We are grateful to the Center for Space Sciences at the University of Texas at Dallas and the U.S. Air Force for providing the DMSP thermal plasma data and to the International GNSS Service (IGS) for the GPS data and products. The authors thank the UML DIDBase (http://umlcar.uml.edu/ DIDBase/), the Australian IPS Radio and Space Service (http://www.ips.gov.au/World_Data_Centre/1/3), and National Institute of Information and Communications and Technology (NICT) of Japan (http://wdc.nict.go.jp/IONO/HP2009/ISDJ/index-E.html) for providing the ionosondes' data. We acknowledge the Physical Oceanography Distributed Active Archive Center, ftp://podaac.jpl.nasa.gov, for the data of GPS receivers and K band measurements from the GRACE satellites. We thank O. Troshichev (Arctic and Antarctic Institute, Russia) and Takashi Kikuchi (STELab, Japan) for the fruitful discussions and comments. This is IPGP contribution 3593.

Alan Rodger thanks the reviewers for their assistance in evaluating this paper.

References

Abdu, M. A., J. R. de Souza, J. H. A. Sobral, and I. S. Batista (2006), Magnetic storm associated disturbance dynamo effects in the low and equatorial latitude ionosphere, in *Recurrent Magnetic Storms: Corotating Solar Wind Streams*, *Geophys. Monogr. Ser.*, vol. 167, edited by B. Tsurutani et al., pp. 283–304, AGU, Washington, D. C.

Astafyeva, E. (2009a), Effects of strong IMF B_z southward events on the equatorial and midlatitude ionosphere, *Ann. Geophys.*, *27*, 1175–1187, doi:10.5194/angeo-27-1175-2009.

Astafyeva, E. I. (2009b), Dayside ionospheric uplift during strong geomagnetic storms as detected by the CHAMP, SAC-C, TOPEX and Jason-1 satellites, *Adv. Space Res.*, *43*, 1749–1756, doi:10.1016/j.asr.2008.09.036.

Astafyeva, E. I., E. L. Afraimovich, and S. V. Voeykov (2008), Generation of secondary waves due to intensive large-scale AGW traveling, *Adv. Space Res.*, *41*(9), 1459–1462, doi:10.1016/j.asr.2007.03.059.

Astafyeva, E., Y. Yasukevich, A. Maksikov, and I. Zhivetiev (2014), Geomagnetic storms, super-storms and their impact on GPS-based navigation, *Space Weather*, *12*, 508–525, doi:10.1002/SW001072.

Balan, N., H. Alleyne, Y. Otsuka, D. Vijaya Lekshmi, B. G. Fejer, and I. McCrea (2009), Relative effects of electric field and neutral wind on positive ionospheric storms, *Earth Planets Space*, *61*, 439–445.

Balan, N., K. Shiokawa, Y. Otsuka, T. Kikuchi, D. Vijaya Lekshmi, S. Kawamura, M. Yamamoto, and G. J. Bailey (2010), A physical mechanism of positive ionospheric storms at low latitudes and midlatitudes, *J. Geophys. Res.*, *115*, A02304, doi:10.1029/2009JA014515.

Balan, N., M. Yamamoto, J. Y. Liu, H. Liu, and H. Lühr (2011), New aspects of thermospheric and ionospheric storms revealed by CHAMP, *J. Geophys. Res.*, *116*, A07305, doi:10.1029/2010JA016399.

Balan, N., J. Y. Liu, Y. Otsuka, S. Tulasi Ram, and H. Lühr (2012), Ionospheric and thermospheric storms at equatorial latitudes observed by CHAMP, ROCSAT, and DMSP, *J. Geophys. Res.*, *117*, A01313, doi:10.1029/2011JA016903.

Basu, S., S. Basu, F. J. Rich, K. M. Groves, E. MacKenzie, C. Coker, Y. Sahai, P. R. Fagundes, and F. Becker-Guedes (2007), Response of the equatorial ionosphere at dusk to penetration electric fields during intense magnetic storms, *J. Geophys. Res.*, *112*, A08308, doi:10.1029/2006JA012192.

Basu, S., S. Basu, J. J. Makela, E. MacKenzie, P. Doherty, J. W. Wright, F. Rich, M. J. Keskinen, R. E. Sheehan, and A. J. Coster (2008), Large magnetic storm-induced nighttime ionospheric flows at midlatitudes and their impacts on GPS-based navigation systems, *J. Geophys. Res.*, *113*, A00A06, doi:10.1029/2008JA013076.

Blanc, M., and A. D. Richmond (1980), The ionospheric disturbance dynamo, *J. Geophys. Res.*, *85*, 1669–1686, doi:10.1029/JA085iA04p01669.
Blewitt, G. (1990), An automatic editing algorithm for GPS data, *Geophys. Res. Lett.*, *17*, 199–202, doi:10.1029/GL017i003p00199.
Bruinsma, S., and R. Biancale (2003), Total densities derived from accelerometer data, *J. Spacecr. Rockets*, *40*(2), 230–236.
Buonsanto, M. J. (1999), Ionospheric storms—A review, *Space Sci. Rev.*, *88*, 563–601.
Danilov, A. D. (2013), Ionospheric F-region response to geomagnetic disturbances, *Adv. Sp. Res.*, *52*(3), 343–366, doi:10.1016/j.asr.2013.04.019.
de Abreu, A. J., et al. (2010), Hemispheric asymmetries in the ionospheric response observed in the American sector during an intense geomagnetic storm, *J. Geophys. Res.*, *115*, A12312, doi:10.1029/2010JA015661.
Doornbos, E., J. van den IJssel, H. Lühr, M. Förster, and G. Koppenwallner (2010), Neutral density and crosswind determination from arbitrarily oriented multiaxis accelerometers on satellites, *J. Spacecr. Rockets*, *47*(4), 580–589, doi:10.2514/1.48114.
Echer, E., W. D. Gonzalez, B. T. Tsurutani, and A. L. C. Gonzalez (2008), Interplanetary conditions causing intense geomagnetic storms ($Dst <= -100$ nT) during solar cycle 23 (1996–2006), *J. Geophys. Res.*, *133*, A05221, doi:10.1029/JA012744.
Fejer, B. G., J. W. Jensen, T. Kikuchi, M. A. Abdu, and J. L. Chau (2007), Equatorial ionospheric electric fields during the November 2004 magnetic storm, *J. Geophys. Res.*, *112*, A10304, doi:10.1029/2007JA012376.
Foster, J. C., and A. J. Coster (2007), Conjugate localized enhancement of total electron content at low latitudes in the American sector, *J. Atmos. Sol. Terr. Phys.*, *69*, 1241–1252.
Fuller-Rowell, T. J. (2011), Storm-time response of the thermosphere-ionosphere system, in *Aeronomy of the Earth's Atmosphere and Ionosphere*, *IAGA Spec. Sopron Book Ser.*, vol. 2, edited by M. A. Abdu, D. Pancheva, and A. Bhattacharyya, chap. 32, pp. 419–435, Springer, doi:10.1007/978-94-007-0326-1_32.
Fuller-Rowell, T. J., M. V. Codrescu, R. J. Moffett, and S. Quegan (1994), Response of the thermosphere and ionosphere to geomagnetic storms, *J. Geophys. Res.*, *99*, 3893–3914, doi:10.1029/93JA02015.
Fuller-Rowell, T. J., A. Richmond, and N. Maruyama (2008), Global modeling of storm-time dynamics and electrodynamics, in *Midlatitude Ionospheric Dynamics and Disturbances*, *Geophys. Monogr. Ser.*, vol. 181, edited by P. M. Kintner Jr. et al., pp. 187–200, AGU, Washington, D. C.
Goncharenko, L. P., J. C. Foster, A. J. Coster, C. Huang, N. Aponte, and L. J. Paxton (2007), Observations of a positive storm phase on September 10, 2005, *J. Atmos. Sol. Terr. Phys.*, *69*, 1253–1272.
Hofmann-Wellenhof, B. (2001), *Global Positioning System: Theory and Practice*, Springer, New-York.
Huang, C.-S., J. C. Foster, and M. C. Kelley (2005a), Long-duration penetration of the interplanetary electric field to the low-latitude ionosphere during the main phase of magnetic storms, *J. Geophys. Res.*, *110*, A11309, doi:10.1029/2005JA011202.
Huang, C.-S., J. C. Foster, L. P. Goncharenko, P. J. Erickson, and W. Rideout (2005b), A strong positive phase of ionospheric storms observed by the Millstone Hill incoherent scatter radar and global GPS network, *J. Geophys. Res.*, *110*, A06303, doi:10.1029/2004JA010865.
Jakowski, N., S. M. Stankov, and D. Klaehn (2005), Operational space weather service for GNSS precise positioning, *Ann. Geophys.*, *23*, 3071–3079.
Karpachev, A. T., L. Z. Biktash, and T. Maruyama (2007), The high-latitude ionosphere structure on 22 March 1979 magnetic storm from multisatellite and ground-based observations, *Adv. Space Res.*, *40*, 1852–1857, doi:10.1016/j.asr.2007.04.088.
Kelley, M. C. (2009), *The Earth's Ionosphere: Electrodynamics and Plasma Physics*, 2nd ed., Elsevier, New York.
Kelley, M. C., J. J. Makela, J. L. Chau, and M. J. Nicolls (2003), Penetration of the solar wind electric field into the magnetosphere/ionosphere system, *Geophys. Res. Lett.*, *30*(4), 1158, doi:10.1029/2002GL016321.
Kelley, M. C., M. N. Vlasov, J. C. Foster, and A. J. Coster (2004), A quantitative explanation for the phenomenon known as storm-enhanced density, *Geophys. Res. Lett.*, *31*, L19809, doi:10.1029/2004GL020875.
Kelley, M. C., R. R. Ilma, and G. Crowley (2009), On the origin of pre-reversal enhancement of the zonal equatorial electric field, *Ann. Geophys.*, *27*, 2053–2056.
Kikuchi, T., T. Araki, H. Maeda, and K. Maekawa (1978), Transmission of polar electric fields to the equator, *Nature*, *273*, 650–651.
Kikuchi, T., K. K. Hashimoto, and K. Nozaki (2008), Penetration of magnetospheric electric fields to the equator during a geomagnetic storm, *J. Geophys. Res.*, *113*, A06214, doi:10.1029/2007JA012628.
Lazutin, L. L., M. I. Panasyuk, and N. Hasebe (2011), Acceleration and losses of energetic protons and electrons during magnetic storm on August 30–31, 2004, *Cosmic Res.*, *49*(1), 38–44.
Lazutin, L., et al. (2008), Comparative analysis of the energetic electron and solar proton dynamics during strong geomagnetic storms, *Physics of Auroral Phenomena*, *Proc. XXXI Annual Seminar*, Apatity, Russia.
Lazutin, L., Y. I. Logachev, E. A. Muravieva, and V. L. Petrov (2012), Relaxation of electron and proton radiation belts of the Earth after strong magnetic storms, *Cosmic Res.*, *50*(1), 3–14.
Liu, H., and H. Lühr (2005), Strong disturbance of the upper thermospheric density due to magnetic storms: CHAMP observations, *J. Geophys. Res.*, *110*, A09S29, doi:10.1029/2004JA010908.
Liu, H., H. Lühr, V. Henize, and W. Köhler (2005), Global distribution of the thermospheric total mass density derived from CHAMP, *J. Geophys. Res.*, *110*, A04301, doi:10.1029/2004JA010741.
Lu, G., L. P. Goncharenko, A. D. Richmond, R. G. Roble, and N. Aponte (2008), A dayside ionospheric positive storm phase driven by neutral winds, *J. Geophys. Res.*, *113*, A08304, doi:10.1029/2007JA012895.
Lu, G., L. Goncharenko, M. J. Nicolis, A. Maute, A. Coster, and L. J. Paxton (2012), Ionospheric and thermospheric variations associated with prompt penetration electric fields, *J. Geophys. Res.*, *117*, A08312, doi:10.1029/2012JA017769.
Ma, G., and T. Maruyama (2003), Derivation of TEC and estimation of instrumental biases from GEONET in Japan, *Ann. Geophys.*, *2083–2093*.
Mannucci, A. J., B. T. Tsurutani, B. A. Iijima, A. Komjathy, A. Saito, W. D. Gonzalez, F. L. Guarnieri, J. U. Kozyra, and R. Skoug (2005), Dayside global ionospheric response to the major interplanetary events of October 29–30 2003 "Halloween Storms," *Geophys. Res. Lett.*, *32*, L12S02, doi:10.1029/2004GL021467.
Mannucci, A. J., B. T. Tsurutani, M. A. Abdu, W. D. Gonzalez, A. Komjathy, E. Echer, B. A. Iijima, G. Crowley, and D. Anderson (2008), Superposed epoch analysis of the dayside ionospheric response to four intense geomagnetic storms, *J. Geophys. Res.*, *113*, A00A02, doi:10.1029/2007JA012732.
Mannucci, A. J., B. T. Tsurutani, M. C. Kelley, B. A. Iijima, and A. Komjathy (2009), Local time dependence of the prompt ionospheric response for the 7, 9, and 10 November 2004 superstorms, *J. Geophys. Res.*, *114*, A10308, doi:10.1029/2009JA014043.
Mannucci, A. J., G. Crowley, B. T. Tsurutani, O. P. Verkhoglyadova, A. Komjathy, P. Stephens (2014), Interplanetary magnetic field by control of prompt total electron content increases during superstorms, *J. Atmos. Sol. Terr. Phys.*, doi:10.1016/j.jastp.2014.01.001.
McNamara, L. F., D. L. Cooke, C. E. Valladares, and B. W. Reinisch (2007), Comparison of CHAMP and Digisonde plasma frequencies at Jicamarca, Peru, *Radio Sci.*, *42*, RS2005, doi:10.1029/2006RS003491.
Ngwira, C. M., L.-A. McKinnell, P. J. Cilliers, and A. J. Coster (2012), Ionospheric observations during the geomagnetic storm events on 24–27 July 2004: Long-duration positive storm effects, *J. Geophys. Res.*, *117*, A00L02, doi:10.1029/2011JA016990.

Paznukhov, V. V., D. Altadill, and B. W. Reinisch (2009), Experimental evidence for the role of the neutral wind in the development of ionospheric storms in midlatitudes, *J. Geophys. Res.*, *114*, A12319, doi:10.1029/2009JA014479.
Pedatella, N. M., J. Lei, K. M. Larson, and J. M. Forbes (2009), Observations of the ionospheric response to the 15 December 2006 geomagnetic storm: Long-duration positive storm effect, *J. Geophys. Res.*, *114*, A12313, doi:10.1029/2009JA014568.
Pi, X., A. J. Mannucci, U. J. Lindqwister, and C. M. Ho (1997), Monitoring of global ionospheric irregularities using the worldwide GPS network, *Geophys. Res. Lett.*, *24*, 2283–2286, doi:10.1029/97GL02273.
Ping, J., K. Matsumoto, K. Heki, A. Saito, P. Callahan, L. Potts, and C. K. Shum (2004), Validation of Jason-1 Nadir ionosphere using GEONET, *Mar. Geod.*, *27*(3-4), 741–752, doi:10.1080/01490410490889049.
Prölls, G. (1995), Ionospheric F-region storms, in *Handbook of Atmospheric Electrodynamics*, vol. 2, edited by H. Volland, pp. 195–248, CRC Press, Boca Raton, Fla.
Rama Rao, P. V. S., S. Gopi Krishna, J. Vara Prasad, S. N. V. S. Prasad, D. S. V. V. D. Prasad, and K. Niranjan (2009), Geomagnetic storm effects on GPS based navigation, *Ann. Geophys.*, *27*, 2101–2110.
Reigber, C., H. Lühr, and P. Schwintzer (2002), CHAMP mission status, *Adv. Space Res.*, *30*(2), 129–134.
Reinisch, B. W., X. Huang, I. A. Galkin, V. Paznukhov, and A. Kozlov (2005), Recent advances in real-time analysis of ionograms and ionospheric drift measurements with digisondes, *J. Atmos. Sol. Terr. Phys.*, *67*, 1054–1062.
Rich, F. J., and M. Hairston (1994), Large-scale convection patterns observed by DMSP, *J. Geophys. Res.*, *99*, 3827–3844, doi:10.1029/93JA03296.
Richmond, A. D., and Y. Kamide (1988), Mapping of ionospheric electro-dynamic features of the high-latitude ionosphere from localized observations, *J. Geophys. Res.*, *93*, 5741–5759, doi:10.1029/JA093iA06p05741.
Richmond, A., and G. Lu (2000), Upper-atmospheric effects of magnetic storms: A brief tutorial, *J. Atmos. Sol. Terr. Phys.*, *62*, 1115–1127.
Sastri, J. H. (1982), Post-sunset behaviour of the equatorial anomaly in the Indian sector, *Indian J. Radio Space Phys.*, *11*, 33–37.
Sica, R. J., and R. W. Schunk (1990), Interpreting vertical plasma drift in the mid-latitude ionosphere using ionosonde measurements, *J. Atmos. Terr. Phys.*, *38*, 1567–1571.
Troshichev, O. A., V. G. Andrezen, S. Vennerstrøm, and E. Friis-Christensen (1988), Magnetic activity in the polar cap: A new index, *Planet. Space Sci.*, *36*, 1095.
Troshichev, O., A. Janzhura, and P. Stauning (2006), Unified PCN and PCS indices: Method of calculation, physical sense, and dependence on the IMF azimuthal and northward components, *J. Geophys. Res.*, *111*, A05208, doi:10.1029/2005JA011402.
Tsunomura, S. (1999), Numerical analysis of global ionospheric current system including the effect of equatorial enhancement, *Ann. Geophys.*, *17*, 692–706.
Tsurutani, B., et al. (2004), Global dayside ionospheric uplift and enhancement associated with interplanetary electric fields, *J. Geophys. Res.*, *109*, A08302, doi:10.1029/2003JA010342.
Tsurutani, B. T., et al. (2006), The dayside ionospheric "superfountain" (DIS), plasma transport and other consequences, *Proceedings of the ILWS Workshop 2006*, pp. 384–388, Goa, India, 19-24 Feb.
Tsurutani, B. T., O. P. Verkhoglyadova, A. J. Mannucci, T. Araki, A. Saito, T. Tsuda, and K. Yumoto (2007), Oxygen ion uplift and satellite drag effect during the 30 October 2003 daytime superfountain effect, *Ann. Geophys.*, *25*, 569–574.
Tsurutani, B. T., et al. (2008), Prompt penetration electric fields (PPEFs) and their ionospheric effects during the great magnetic storm of 30–31 October 2003, *J. Geophys. Res.*, *113*, A05311, doi:10.1029/2007JA012879.
Vlasov, M., M. C. Kelley, and H. Kil (2003), Analysis of satellite and ground-based observations of F-region behavior during the great magnetic storm of July 15, 2000, *J. Atmos. Sol.Terr. Phys.*, *65*, 1223–1234.
Woodman, R. F. (1970), Vertical drift velocities and east-west electric fields at the magnetic equator, *J. Geophys. Res.*, *75*, 6249–6259, doi:10.1029/JA075i031p06249.
Xiong, C., J. Park, H. Lühr, C. Stolle, and S. Y. Ma (2010), Comparing plasma bubble occurrence rates at CHAMP and GRACE altitudes during high and low solar activity, *Ann. Geophys.*, *28*, 1647–1658, doi:10.5194/angeo-28-1647-2010.
Yasukevich, Y. V., E. L. Afraimovich, K. S. Palamarchuk, and P. V. Tatarinov (2009), Testing of the international reference ionosphere model using the data of dual-frequency satellite altimeters TOPEX/Poseidon and Jason-1, *Radiophys. Quantum Electron.*, *52*(5–6), 341–353.
Yizengaw, E., M. B. Moldwin, P. L. Dyson, and T. J. Immel (2005), Southern Hemisphere ionosphere and plasmasphere response to the interplanetary shock event of 29–31 October 2003, *J. Geophys. Res.*, *110*, A09S30, doi:10.1029/2004JA010920.
Yizengaw, E., M. B. Moldwin, A. Komjathy, and A. J. Mannucci (2006), Unusual topside ionospheric density response to the November 2003 superstorm, *J. Geophys. Res.*, *111*, A02308, doi:10.1029/2005JA011433.
Yizengaw, E., M. B. Moldwin, D. Galvan, B. A. Iijima, A. Komjathy, and A. J. Mannucci (2008), Global plasmaspheric TEC and its relative contribution to GPS TEC, *J. Atmos. Sol. Terr. Phys.*, *70*, 1541–1548.
Yue, X., W. S. Schreiner, D. C. Hunt, C. Rocken, and Y.-H. Kuo (2011), Quantitative evaluation of the low Earth orbit satellite based slant total electron content determination, *Space Weather*, *9*, S09001, doi:10.1029/2011SW000687.
Zakharenkova, I. E., A. Krankowski, I. I. Shagimuratov, Y. V. Cherniak, A. Krypiak-Gregorcyk, P. Wielgosz, and A. F. Lagovsky (2012), Observation of the ionospheric storm of October 11, 2008 using FORMOSAT-3/COSMIC data, *Earth Planets Space*, *64*, 505–512.
Zakharenkova, I. E., I. V. Cherniak, A. Krankowski, and I. I. Shagimuratov (2014), Cross-hemisphere comparison of mid-latitude ionospheric variability during 1996–2009: Juliusruh vs. Hobart, *Adv. Space Res.*, *53*(2), 175–189, doi:10.1016/j.asr.2013.10.027.
Zakharenkova, I. E., and E. Astafyeva (2015), Topside ionospheric irregularities as seen from multi-satellite observations, *J. Geophys. Res. Space Physics*, doi:10.1002/2014JA020330.